remote sensing

MDPI

Article

Power Pylon Reconstruction from Airborne LiDAR Data Based on Component Segmentation and Model Matching

Yiya Qiao [1,2,3], Xiaohuan Xi [1,*], Sheng Nie [1], Pu Wang [1,2], Hao Guo [3] and Cheng Wang [1,2]

[1] Key Laboratory of Digital Earth Science, Aerospace Information Research Institute, Chinese Academy of Sciences, Beijing 100094, China
[2] College of Resources and Environment, University of Chinese Academy of Sciences, Beijing 100049, China
[3] College of Land Science and Technology, China Agricultural University, Beijing 100083, China
* Correspondence: xixh@aircas.ac.cn

Abstract: In recent years, with the rapid growth of State Grid digitization, it has become necessary to perform three-dimensional (3D) reconstruction of power elements with high efficiency and precision to achieve full coverage when simulating important transmission lines. Limited by the performance of acquisition equipment and the environment, the actual scanned point cloud usually has problems such as noise interference and data loss, presenting a great challenge for 3D reconstruction. This study proposes a model-driven 3D reconstruction method based on Airborne LiDAR point cloud data. Firstly, power pylon redirection is realized based on the Principal Component Analysis (PCA) algorithm. Secondly, the vertical and horizontal distribution characteristics of the power pylon point cloud and the graphical characteristics of the overall two-dimensional (2D) orthographic projection are analyzed to determine segmentation positions and the key segmentation position of the power pylon. The 2D alpha shape algorithm is adopted to obtain the pylon body contour points, and then the pylon feature points are extracted and corrected. Based on feature points, the components of original pylon and model pylon are registered, and the distance between the original point cloud and the model point cloud is calculated at the same time. Finally, the model with the highest matching degree is regarded as the reconstructed model of the pylon. The main advantages of the proposed method include: (1) identifying the key segmentation position according to the graphical characteristics; (2) for some pylons with much missing data, the complete model can be accurately reconstructed. The average RMSE (Root-Mean-Square Error) of all power pylon components in this study was 15.4 cm. The experimental results reveal that the effects of power pylon structure segmentation and reconstruction are satisfactory, which provides method and model support for digital management and security analysis of transmission lines.

Keywords: Airborne LiDAR; model-driven; power pylon; three-dimensional reconstruction; point cloud registration

Citation: Qiao, Y.; Xi, X.; Nie, S.; Wang, P.; Guo, H.; Wang, C. Power Pylon Reconstruction from Airborne LiDAR Data Based on Component Segmentation and Model Matching. *Remote Sens.* **2022**, *14*, 4905. https://doi.org/10.3390/rs14194905

Academic Editors: Wei Yao, Wenbing Tao and Jie Shao

Received: 31 August 2022
Accepted: 26 September 2022
Published: 30 September 2022

1. Introduction

Electrical energy is an indispensable source for daily human life; it is vital to sustain its uninterrupted generation, transmission, and distribution [1,2]. However, the power grid has long transmission distances reaching wide areas, which makes it exposed to the complex and varying geographical environment [3]. Hence, bad weather conditions, such as snowstorms, hails, and typhoons or natural disasters (e.g., earthquakes, floods, and landslides [4]) have certain impacts on the reliability of the transmission lines [5]. To ensure the stable and efficient operation of the power grids, it is necessary to monitor the high-voltage lines regularly [6–8]. As one of the key components of transmission lines, power pylons are directly related to the security of high-voltage lines [9,10]. Power pylon monitoring includes checking whether the pylon structure is complete, deformed, or inclined, and whether the pylon base is stable. Conventional methods include artificial

visual observation, instrument measurement, and aerial photogrammetry, which are often inefficient, difficult, or it is impossible to achieve monitoring due to various limitations and the lack of three-dimensional (3D) information.

Airborne LiDAR (Light Detection and Ranging) technology, as a new technique to obtain 3D spatial data, has been widely used in many fields, such as forestry resources, digital city, and power inspection, due to its directness, high precision, and high efficiency. It is not restricted by complex terrain conditions and can obtain high-density and high-precision 3D point cloud information of the power pylon directly and quickly [11–14]. Through data processing, the 3D vector or the true 3D digital model of the power pylon is constructed to restore the real shape of transmission lines, which provides basic data and model support for the digitization, visualization, and automation of power grid facilities.

1.1. Related Works

In recent years, several researchers have studied the classification and 3D reconstruction of transmission lines and ground features using Airborne LiDAR point cloud data. However, the research on automatic modeling of power pylons is relatively limited. Due to the complexity of the pylon structure, the diversity of the pylon type [8], and the occlusion by ground objects, the data may be missing or the point density may not be high enough during the actual scanning, which poses challenges to accurate and rapid reconstruction. Currently, there are many methods for power pylon 3D reconstruction based on laser point clouds, which can be generally divided into three categories according to their processing strategy: (i) data-driven, (ii) model-driven, and (iii) hybrid-driven [8]. The reconstruction strategy of the data-driven method is often bottom-up, without making assumptions about the shape and style of the object in advance, but commencing with the data directly. Han [15] first extracted the power pylon point clouds by using the connection points of the power line pairs, and then used the binary image contour line tracking method to track lines followed by reconstructing pylons according to the tracked lines. This method was limited to the data quality, such as the point density and distribution, required by the data-driven strategy [16]. The model-driven method adopts a top-down process contrary to its data-driven counterpart, in which the model library needs to be defined in advance. Then, the best matching model is searched to complete the reconstruction. Yu et al. [17] proposed a model-driven power pylon modeling method. They established a local coordinate system for the pylon, captured the key points of the pylon through manual semi-interaction, and matched the models in the model library to obtain the best matching model. This method ensured the integrity of the established model, but the modeling process required some manual intervention. Li et al. [18] divided the pylon into three parts: the foot, the body, and the head. They determined the pylon head type by SVM (Support Vector Machine) classification method and reconstructed the head with a pre-build head model library. The pylon body was reconstructed by calculating intersection lines of the fitted side planes. They proposed a 3D pylon reconstruction method based on the constructed parametric pylon model. Experiments suggested that the pylon head and body can be reconstructed automatically. However, interactive operation was required for pylon foot reconstruction. Guo et al. [7] proposed a new method for the accurate reconstruction of power pylons. They defined the energy function as composed of two terms, combined with Markov Chain Monte Carlo (MCMC) and Simulated Annealing (SA) algorithms, to determine the optimal parameters in the process of optimizing the energy function. The maximum distance from the laser points to the models was 0.32 m. This strategy is robust in terms of data quality, but it takes a long time when required to estimate a large number of parameters. The hybrid-driven strategy combines two methods, data-driven and model-driven, and introduces constraints taken from prior knowledge, such as symmetry, orthogonality, and coplanarity, to achieve model optimization. Generally, different strategies are adopted for different blocks and the modeling requirements of each structure are considered, which can improve the modeling accuracy. For example, Zhou et al. [8] divided the power pylon into two parts (pylon body and pylon head) by analyzing the local

maximum point density and local minimum length. They reconstructed the pylon body by fitting edge lines using RANSAC (Random Sample Consensus) algorithm, identified the pylon type, estimated parameters by shape context algorithm, and simulated annealing algorithm, respectively. This method can effectively reconstruct the main structure of pylon, but it lacks the representation of the internal structure. Chen et al. [14] proposed to reconstruct complex upper structures by establishing an a priori abstract template structure, and to reconstruct inverted triangular pyramid lower structures and quadrangular frustum pyramid middle structures based on data fitting. Experiments have shown that this method improved reconstruction efficiency and 3D models can display part of the internal structure of the pylon. However, when faced with a pylon missing data, the model reconstructed by this method is prone to incompletion. In summary, although the model-driven strategy is limited by the model library, it has great advantages in dealing with missing data and describing model details.

1.2. Contributions

This study analyzes the vertical and horizontal distribution characteristics of the power pylon point cloud and graphical characteristics of the overall 2D orthographic projection. Concavity vs. convexity is introduced as a new feature to identify the key segmentation position. It proposes an automatic model-driven 3D reconstruction method of the pylon based on component segmentation. The applicability and accuracy of the proposed method are experimentally verified. This study also demonstrates the great potential of model matching methods for reconstructing complete and detailed models, particularly for some pylons with missing data.

1.3. Overview

The study is organized as follows. Section 2 elaborates on the experimental data. Section 3 explains the novel model-driven reconstruction method that is proposed in this study. In addition to the parameter settings, the segmentation and reconstruction results are presented in Section 4. Section 5 discusses the influence of three main factors on segmentation and reconstruction. Finally, Section 6 provides the conclusions and puts forward future work.

2. Experimental Data

The experimental data relating to the transmission channel were collected in 2017 by a LiDAR system, named Riegl VUX-1UAV, which was located in an ultra-high-voltage transmission corridor of the State Grid in Anhui Province, China. The UAV flew at the speed of 8 m/s and about 40 m high above the power lines. Table 1 shows the technical specifications of the LiDAR system.

Table 1. Technical specifications of the LiDAR system.

Parameter	Index
Field of view	330°
Pulse repetition frequency	550 kHz
Maximum scan speed	200 scans/s
Beam divergence	0.5 mrad
Accuracy/precision	10 mm/5 mm
Max. range: target reflectivity 60%	920 m
Max. range: target reflectivity 20%	550 m
Average point density	100 pts/m^2

Hollow structure and T-support structure are two common structures of the power pylon head. Based on this, power pylons can be mainly divided into type-T pylons and type-O pylons, which are principal research objects in this study. Six different types of

power pylons, (a–f), were finely extracted with complete structure and low noise. Figure 1 shows the pylon point clouds. Details are provided in Table 2.

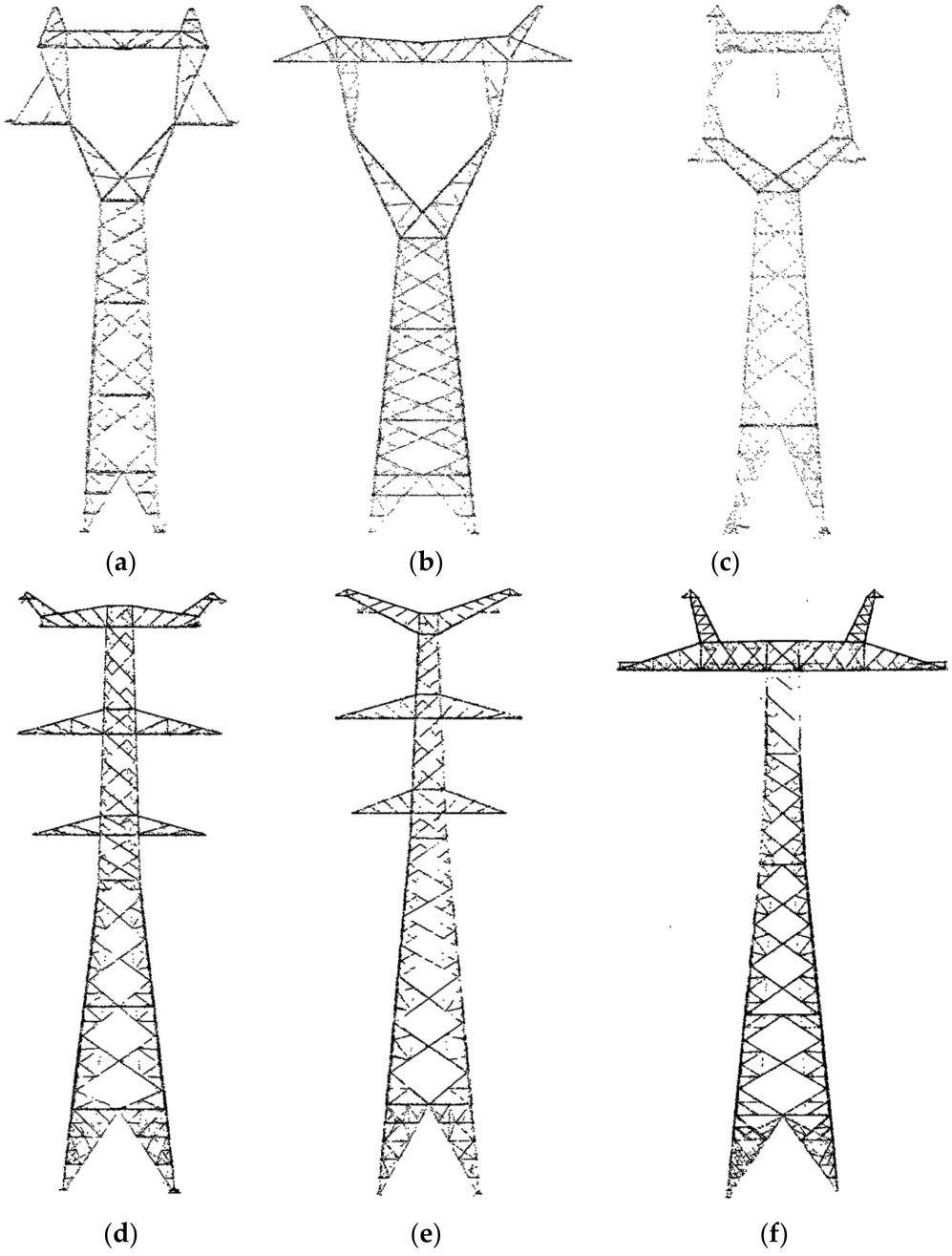

Figure 1. Power pylon point clouds. (**a**–**c**) Pylons of type-O; (**d**–**f**) pylons of type-T.

Table 2. Details of the power pylon point clouds.

Pylon Number	Number of Points	Length of the Pylon (m)	Width of the Pylon (m)	Height of the Pylon (m)
a	6163	15.155	4.376	34.134
b	7489	24.464	7.011	43.352
c	3033	9.954	5.865	30.012
d	16,423	22.695	13.219	65.552
e	10,922	20.424	11.446	66.502
f	25,775	47.590	16.351	87.702

Models of common components which have been built and their feature point coordinates were stored in the model library according to the categories of cross-arm, pylon head, and quadrangular frustum pyramid. Figure 2 shows some typical models which have been built.

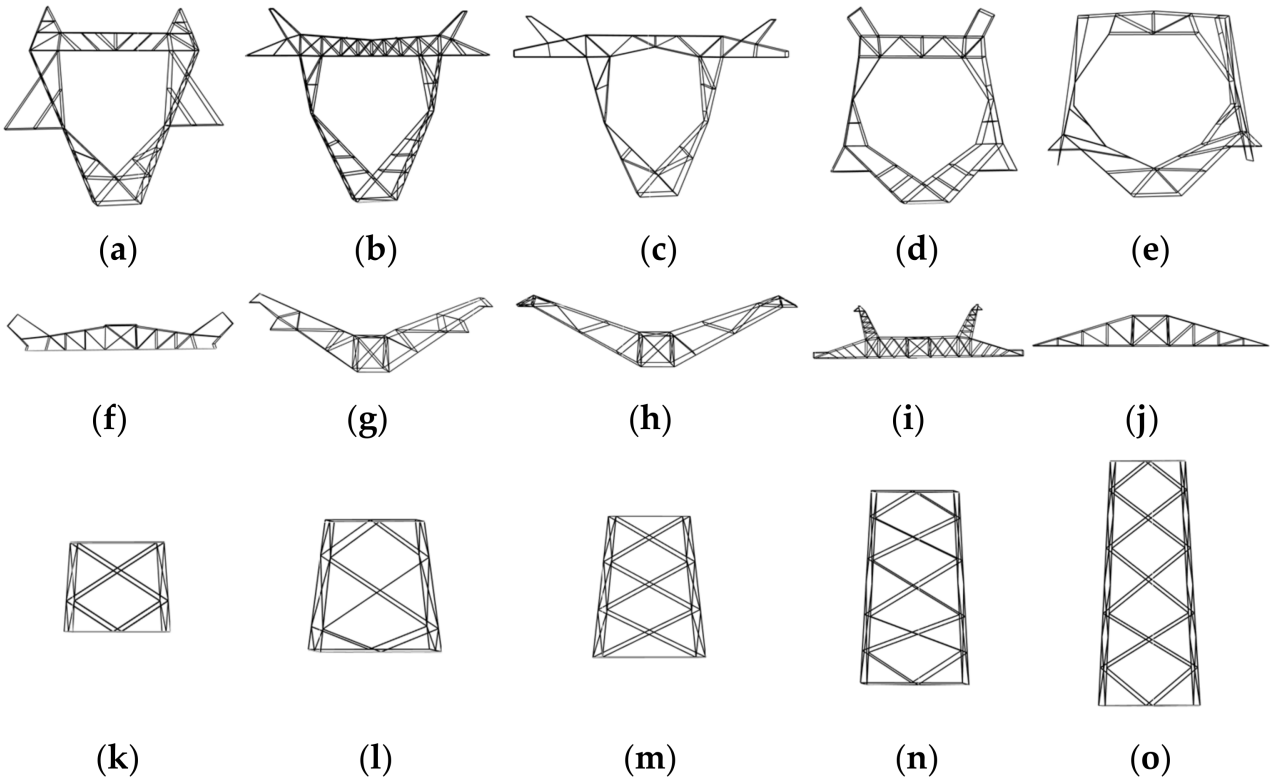

Figure 2. Some typical component models in the model library: (**a**–**e**) models of type-O pylon head; (**f**–**i**) models of type-T pylon head; (**j**) the model of type-T pylon cross arms; (**k**–**o**) models of quadrangular frustum pyramid structure.

3. Methodology

Figure 3 illustrates the processing flowchart of the reconstruction method, divided into the following steps: complete the redirection of the power pylon based on the Principal Component Analysis (PCA) algorithm; analyze the vertical and horizontal distribution characteristics and the graphical characteristics of the overall 2D orthographic projection to finish decomposing key structures of the power pylon (pylon head, pylon body, and pylon foot); identify the pylon type and further divide key structures of the pylon into several components; obtain pylon body contour points, then extract and correct feature points of each component; match the component with models in the model library to find the best matching model.

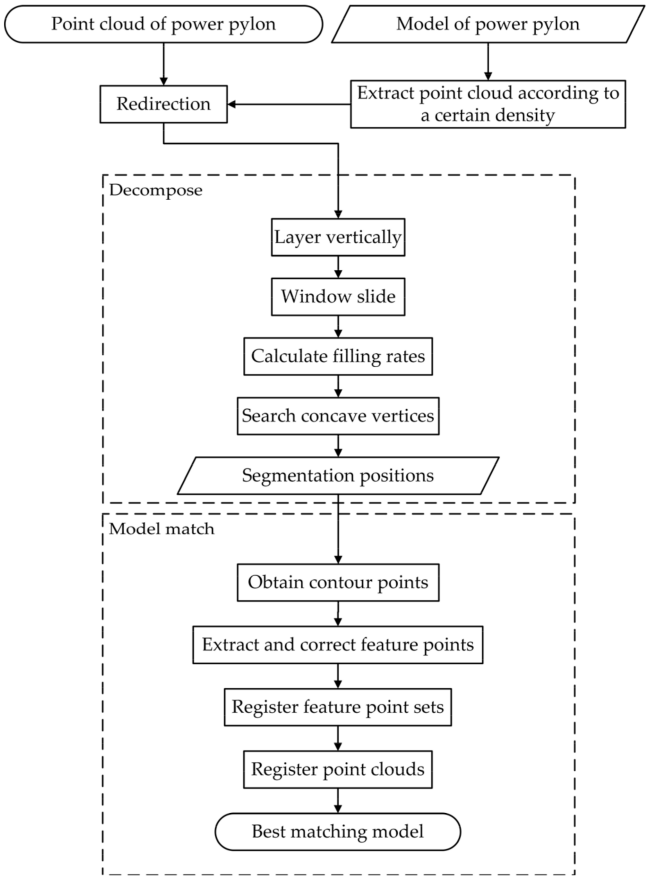

Figure 3. The processing flowchart of the reconstruction method.

3.1. Pylon Redirection

The orientation of the power pylon point cloud on the XY plane is arbitrary, as shown in Figure 4. To make full use of its orthographic projection in extracting local features, the PCA algorithm is used to calculate the rotation angle θ. The pylon is rotated θ degrees around the Z-axis direction to achieve the redirection. The specific steps are as follows:

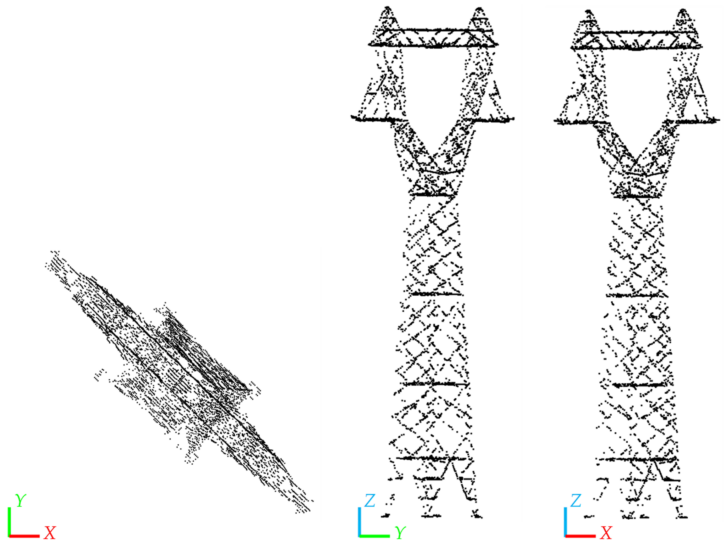

Figure 4. The projections of the pylon on the XY, YZ, and XZ planes.

(1) The orientation of the power pylon on the XY plane is mainly related to its superstructure, here select the point cloud with the Z value above H and project the selected point cloud onto the XY plane;
(2) The PCA algorithm is used to calculate the eigenvalues and eigenvectors of the point cloud after projection, where the eigenvector (v_1, v_2) that corresponds to the smallest eigenvalue is perpendicular to the principal direction of the point cloud at this time;
(3) Equation (1) is used to calculate the rotation angle θ:

$$\theta = \arccos\left(\frac{v_1}{\sqrt{{v_1}^2 + {v_2}^2}}\right) \tag{1}$$

v_1>0, v_2>0, $\theta \in \left(0, \frac{\pi}{2}\right)$; v_1>0, v_2<0, $\theta \in \left(\frac{3\pi}{2}, 2\pi\right)$.

(4) Equation (2) is used to calculate x' and y' coordinates after rotation:

$$\begin{cases} x' = xcos(\theta) + ysin(\theta) \\ y' = ycos(\theta) - xsin(\theta) \end{cases} \tag{2}$$

Figure 5 shows the projections of the pylon after redirection.

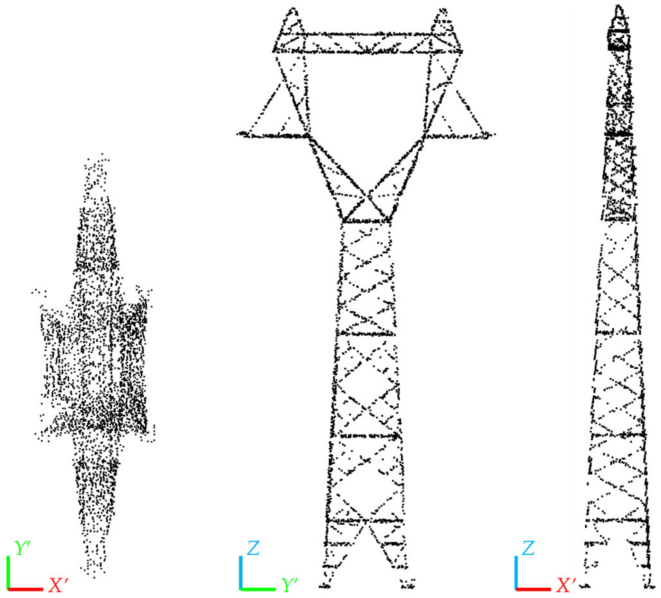

Figure 5. The projections of the pylon on the planes of X′Y′, Y′Z, and X′Z.

3.2. Pylon Structure Segmentation

The types of power pylon vary. Observing the whole pylon structure from top to bottom, it is found that it can usually be divided into three parts: pylon head, pylon body, and pylon foot. The structure of the pylon head is complex, which is the key to distinguishing different pylon types. The pylon body and foot are relatively regular and simple in structure, which can be abstracted as quadrangular frustum pyramids and inverted triangular pyramids. Accurate segmentation of the pylon determines whether the subsequent feature points can be effectively extracted. Feature points play an important role in the registration process. Therefore, pylon structure segmentation is a key step in the reconstruction process. Firstly, determine the segmentation positions of the pylon based on the vertical density and the horizontal filling rate of the pylon point cloud; secondly, traverse the vertices of the constructed polygon and find the concave vertices to determine the key segmentation position that divides pylon head and pylon body; thirdly, identify the pylon type according to the vertical filling rate of the pylon head; finally, divide the pylon into several components, then finish the decomposition of the pylon.

3.2.1. Identification of Segmentation Positions

The point cloud density histogram of the power pylon is generated through the vertical layering of the pylon. Then, a sliding window is used to find the local maximum density layer, and the segmentation positions are further identified based on the horizontal filling rate.

The pylons are layered with a certain interval d_1 along the Z-axis, and the number of points falling into each layer is counted to generate the density histogram of the pylon point cloud. By setting a sliding window W with height D, slide one layer at a time upward from the bottom of the pylon. If the number of points in the middle layer of the sliding window is greater than the number of points in other layers in the window, the middle layer of the window is determined to be the layer with the local maximum density, as shown in Figure 6 (dark green lines).

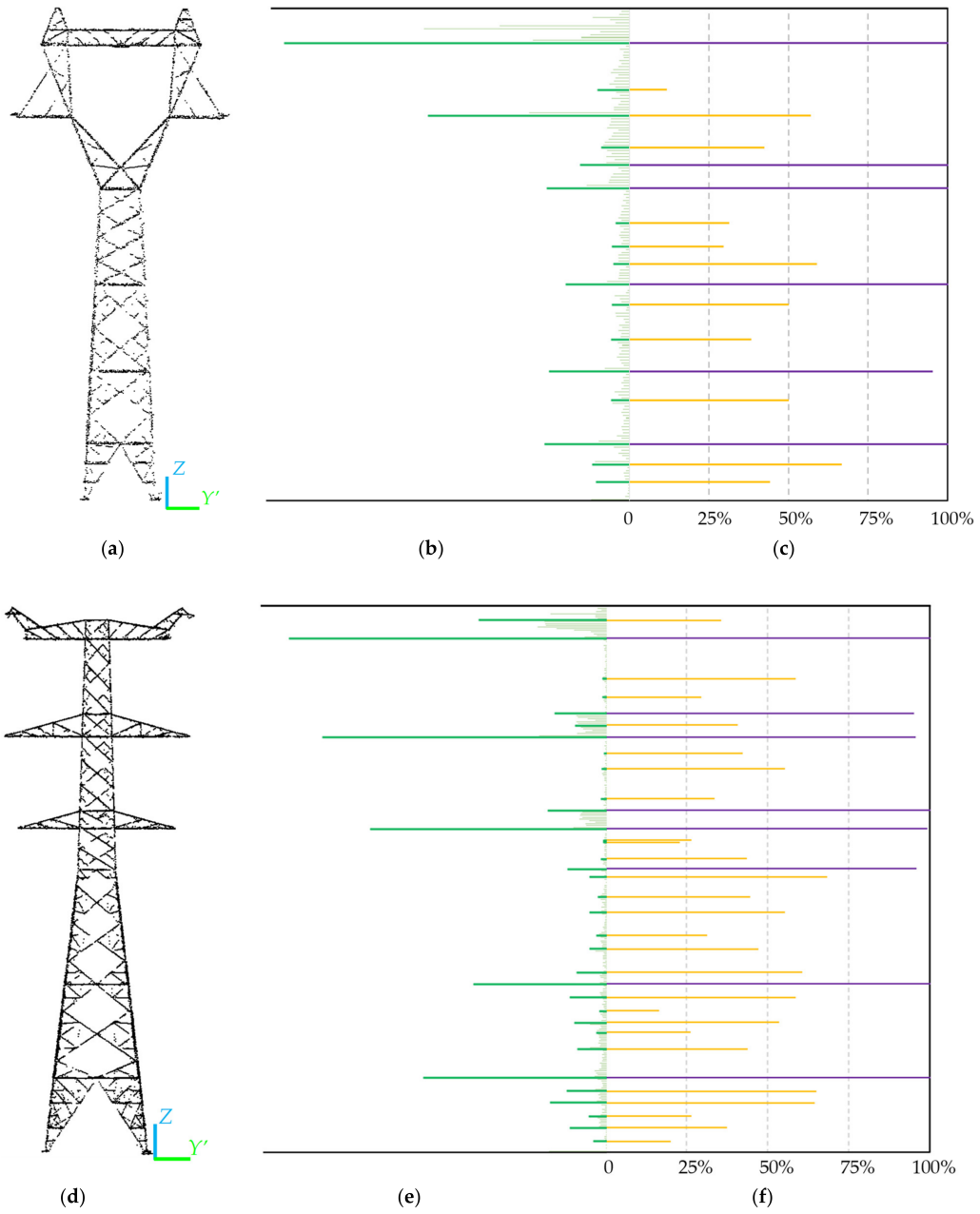

Figure 6. Pylon segmentation position identification: (**a**,**d**) Projections of the pylon on the Y′Z plane; (**b**,**e**) density histograms, and dark green lines are layers with the local maximum density; (**c**,**f**) filling rate histograms, and purple lines are segmentation positions.

In practice, not all layers with the local maximum density correspond to the segmentation positions of the pylon. Obviously, the filling rate of the segmentation positions in the horizontal direction is greater than that of other sections. Therefore, the segmentation positions can be further determined by calculating the filling rates. The calculation process of the filling rate [18] is as follows. The points in each layer are projected onto the X'Y' plane and then divided into N grids at the interval d_2 along the Y'-axis direction, as shown in Figure 7. The number of grids that contain points is counted as n, and n/N is calculated to be the filling rate f of this layer.

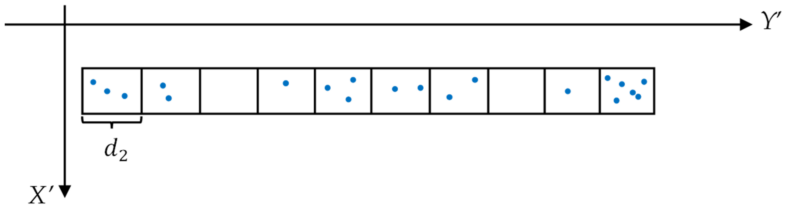

Figure 7. The calculation process of the filling rate.

If the filling rate f of the layer is greater than the threshold value T_f, the middle position of that layer is considered as the segmentation positions S_i (numbered from bottom to top), as shown in Figure 6 (purple lines).

3.2.2. Key Segmentation Position Identification

The segmentation position separating the pylon head and body is defined as the key segmentation position [14]. Projecting the pylon point cloud onto the Y'Z plane, let point P_{ymaxi} be with the largest Y coordinate in the layer corresponding to each segmentation position, as shown in Figure 8a (orange dots). Then, let one point whose Y coordinate is the middle value $((Y_{max} + Y_{\min})/2)$ in the layer corresponding to the segmentation position S_1. Similarly, the other point corresponds to the segmentation position $S_{\max}$, as shown in Figure 8a (blue dots). Connect those points, in turn, to form a closed polygon, as shown in Figure 8b.

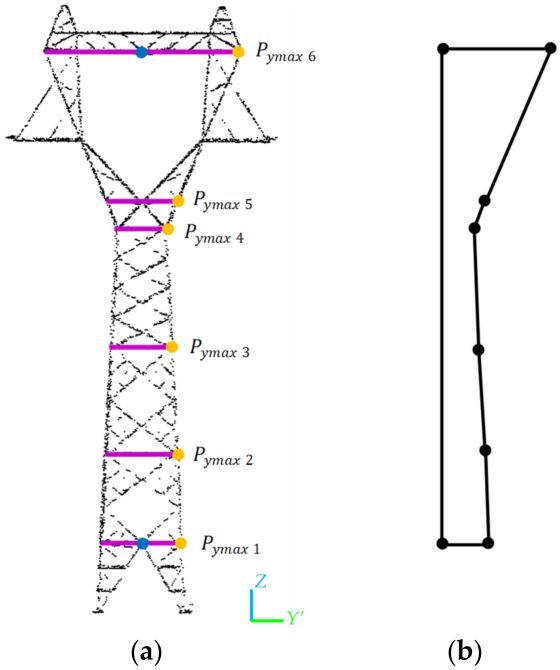

Figure 8. Illustration of the closed polygon construction: (**a**) construction of the closed polygon; (**b**) the result of the closed polygon construction.

By traversing vertices P_{ymaxi} from bottom to top in the counterclockwise direction, the concave vertices of the polygon are obtained by the Vector Product method. As shown in Figure 9a, assume that the coordinate of the vertex v_i is $(0, y_i, z_i)$, the coordinate of the vertex v_{i-1} before that vertex is $(0, y_{i-1}, z_{i-1})$, the coordinate of the vertex v_{i-1} after that vertex is $(0, y_{i+1}, z_{i+1})$, vector $V_1 = (0, y_i - y_{i-1}, z_i - z_{i-1})$, vector $V_2 = (0, y_{i+1} - y_{i-1}, z_{i+1} - z_{i-1})$, and vector $V_3 = V_1 \times V_2$. If the result of the cross product V_3, is positive, its direction is perpendicular to the paper surface, and vertex i is convex; otherwise, it is concave. The green points in Figure 9b are all concave vertices. If angle α_i of the concave vertex is less than the threshold T_α, this vertex will become a candidate point. When the point with the smallest i value among the candidate points is selected, the segmentation position corresponding to that concave vertex becomes the key segmentation position S_k.

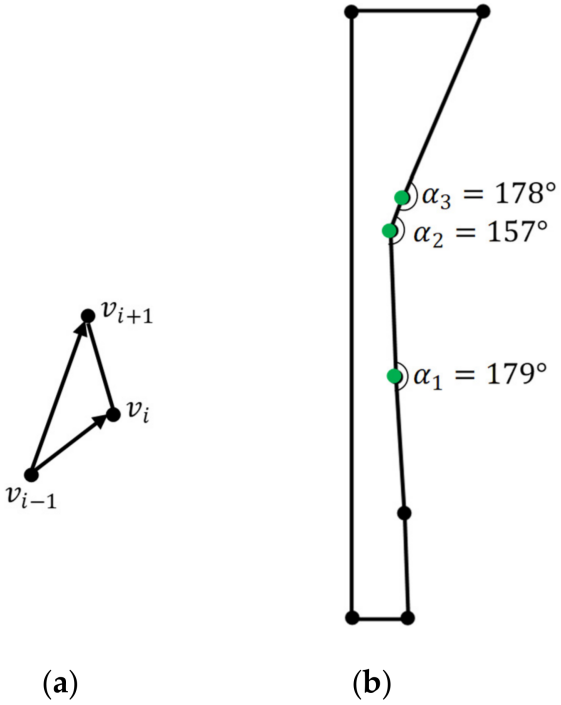

Figure 9. Searching process of polygon concave vertices: (**a**) the cross-product-based concavity vs. convexity determination; (**b**) the concave vertices of the polygon.

The segmentation position S_1 usually separates the pylon body and foot, but sometimes there are special cases, as shown in Figure 10. Those cases can be determined by calculating the vertical distance d_{12} between the segmentation positions S_1 and S_2. To be more specific, the average value of all distance intervals between the adjacent segmentation positions from S_1 to S_k are calculated. If d_{12} is less than the average that is multiplied by the proportional threshold T_r, i.e., d_{12}< (average$\times T_r$), S_1 is abandoned and it is renumbered upward from the segmentation position S_2.

In summary, the pylon segmentation position S_i and the key segmentation position S_k have been determined so far, and the pylon has been divided into three parts: the head, the body, and the foot, as shown in Figure 11.

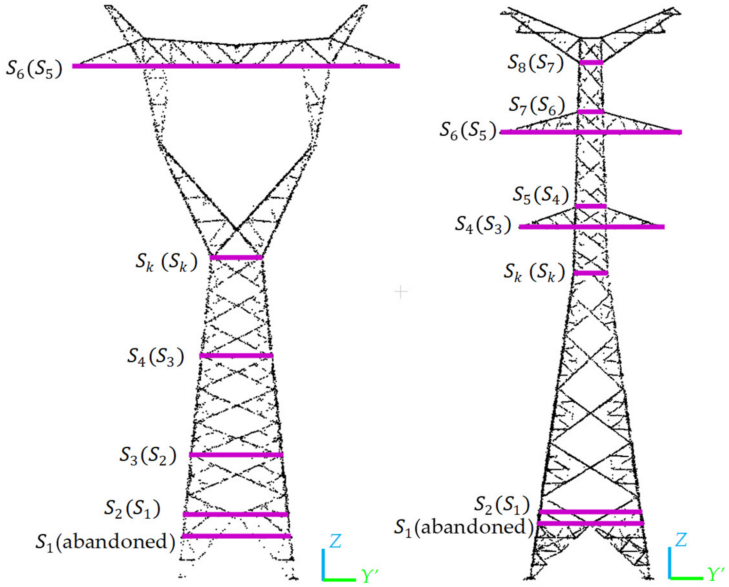

Figure 10. Special cases of segmentation positions. Purple lines are segmentation positions.

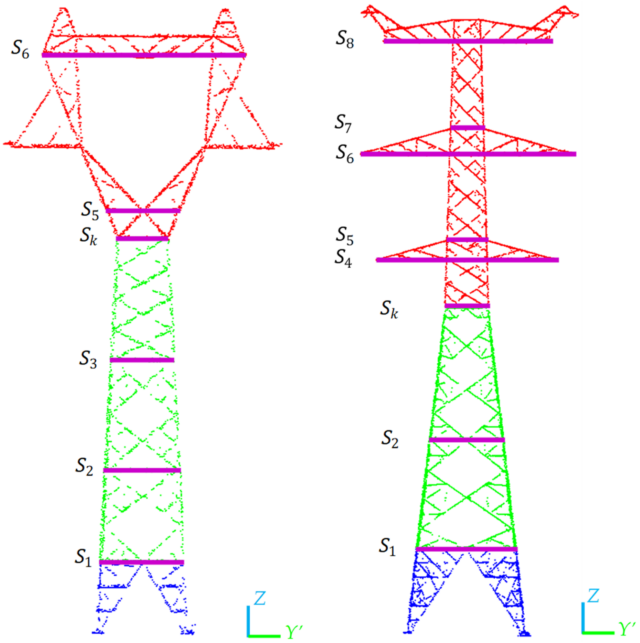

Figure 11. Segmentation positions of the pylon. The red point cloud is the pylon head; the green is the pylon body; the blue is the pylon foot.

3.2.3. Type Identification and Structure Segmentation

The vertical filling rates of type-O pylon and type-T pylon in the blue box areas in Figure 12a,b are obviously different. Each blue box is a rectangle generated by vertically extending upward with the key segmentation position (red lines in Figure 12a,b) as the bottom edge. The pylon heads are layered with the interval d_3 along the Y′-axis direction, then compute the vertical filling rate of each layer. The calculation method of filling rate is similar to that mentioned in Section 3.2.1, except that the value of N which equals the pylon head height divided by d_1 is fixed for a certain pylon.

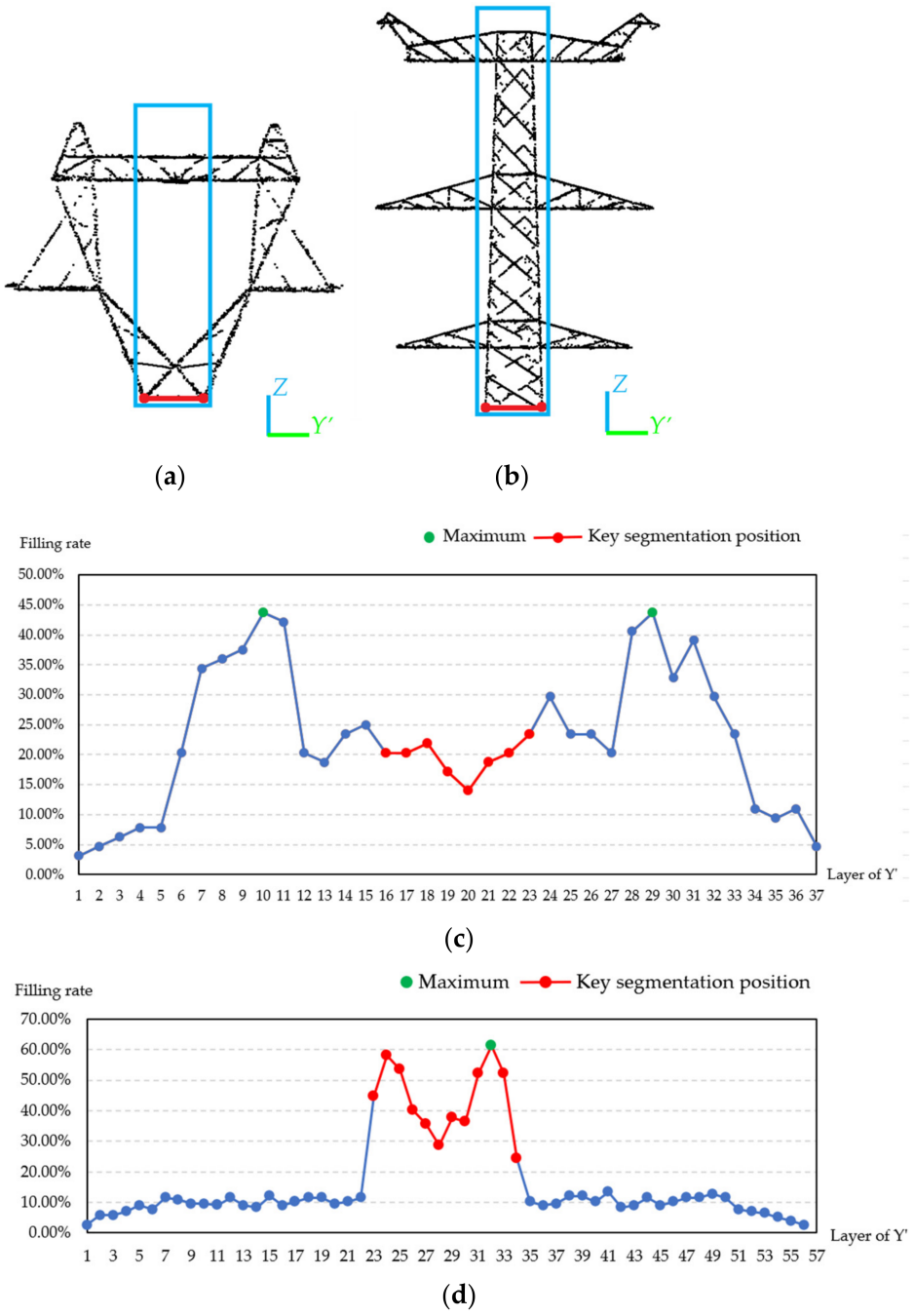

Figure 12. (**a**,**b**) Projections of the pylon head on the Y′Z plane; (**c**,**d**) vertical filling rate histograms, corresponding to type-O pylon head and type-T pylon head, respectively.

If the layer with the largest filling rate is in the blue box area, the pylon is a type-T pylon, as shown in Figure 12d; otherwise it is a type-O pylon, as shown in Figure 12c. If the pylon is a type-T pylon, its head can be further divided into cross arms, quadrangular frustum pyramid structures and head, while the type-O pylon does not need to be subdivided.

The final segmentation results are shown in Figure 13. Pylons are divided into several components.

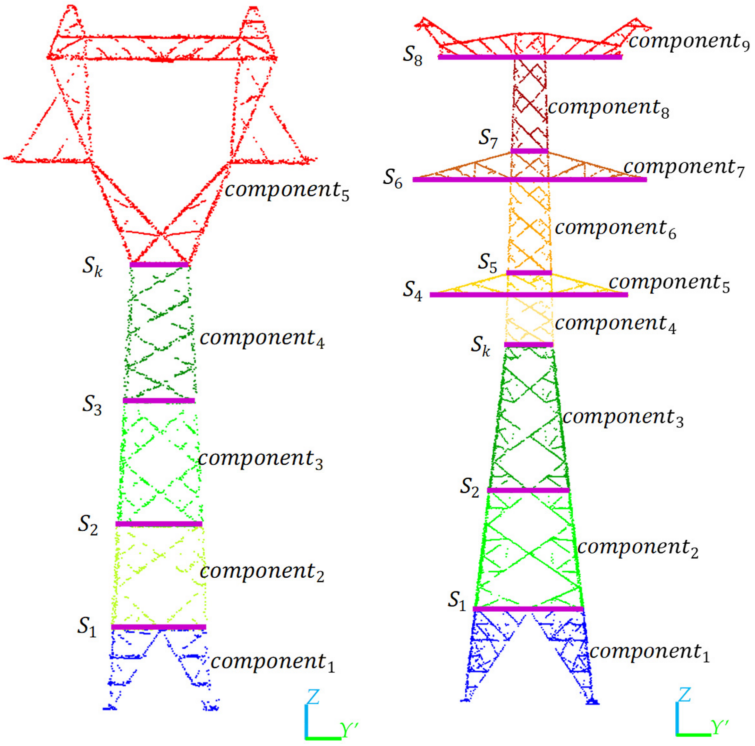

Figure 13. The final segmentation results. Each color represents a component of the pylon.

3.3. Pylon Reconstruction

The feature points are extracted based on the pylon segmentation positions S_i as explained in Section 3.2. The original pylon component feature points are registered with the model pylon component feature points to obtain transformation parameters, which are then utilized to perform the spatial transformation of the model pylon component. Lastly, the model pylon component with the highest matching degree is considered as the reconstruction model.

3.3.1. Extract the Point Cloud Data from the Model

The power pylon model data is in the OBJ format, which needs to be sampled as the point cloud to facilitate the subsequent extraction of feature points and their registration with the original pylon point cloud. As shown in Figure 14, in the rectangular space coordinate system, suppose that point $P_A(x_A, y_A, z_A)$ and point $P_B(x_B, y_B, z_B)$ are the vertices of the line $P_A P_B$ in a pylon model. Then, the line $P_A P_B$ is sampled as points with a sampling interval d_s.

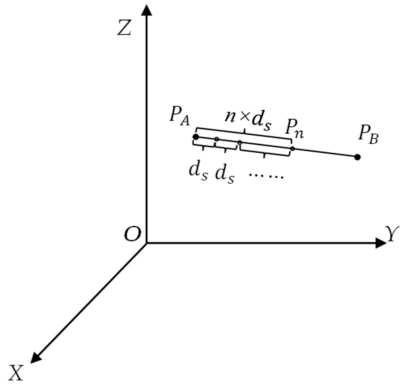

Figure 14. Sampling principle of the pylon model.

The sampling principle is as follows. In the 3D space, the formula of definite proportion and the separated points is used. Supposing that $P_AP_n = \lambda P_nP_B$, and $P_AP_B = P_AP_n + P_nP_B$, the coordinate of the sampling point $P_n(x_n, y_n, z_n)$ can be calculated as Equation (3):

$$\begin{cases} x_n = \frac{x_A + \lambda x_B}{1+\lambda} \\ y_n = \frac{y_A + \lambda y_B}{1+\lambda} \\ z_n = \frac{z_A + \lambda z_B}{1+\lambda} \end{cases} \quad (3)$$

where $\lambda = \frac{n \times d}{distance(P_AP_B) - n \times d}$, and $distance(P_AP_B) = \sqrt{(x_B - x_A)^2 + (y_B - y_A)^2 + (z_B - z_A)^2}$.

When the value of n varies from 1 to N, where N indicates the largest integer that is smaller than the distance $(P_AP_B)/d_s$, the sampling points of the line P_AP_B with a distance interval of d_s are obtained. All the connecting lines in the model are sampled as points according to the above method. The encrypted point cloud can be obtained if combined with the existing vertices in the original model.

3.3.2. Extract and Correct Feature Points

Based on the pylon segmentation positions S_i, the pylon feature points are determined, which are then used for subsequent registration. Traverse all points in the layer corresponding to S_i, and record the maximum value of X coordinate as x_{maxi}, the minimum value of X coordinate as x_{mini}, the maximum value of Y coordinate as y_{maxi}, and the minimum value of Y coordinate as y_{mini}. Take the points as $Feapoint_1(x_{mini}, y_{mini}, z_{s_i})$, $Feapoint_2(x_{mini}, y_{maxi}, z_{s_i})$, $Feapoint_3(x_{maxi}, y_{mini}, z_{s_i})$, and $Feapoint_4(x_{maxi}, y_{maxi}, z_{s_i})$. The point set $Feapoint$ is regarded as the feature point set of the pylon. However, as shown in Figure 15a,b (purple dots in red circles), if boundary points that are located at segmentation positions are missing, there will be some deviation between the extracted feature points and their real positions. To solve this problem, the feature points of the pylon body are extracted by means of the fitting method. Firstly, the pylon body is projected onto the YZ′ plane, and then 2D alpha shape algorithm is used to extract boundary points after down sampling. Secondly, remove points less than Δd away from the upper or lower segmentation position (S_1, S_k), and left boundary and right boundary are divided according to the centroid of pylon, as shown in Figure 16. Then, after extracting the boundary points, the RANSAC algorithm is applied to fit the line equations, respectively. Finally, z_{s_i} are substituted into the equation to obtain y'_{mini} and y'_{maxi}. Similarly, project the pylon body onto the XZ′ plane, and then repeat above steps to obtain x'_{mini} and x'_{maxi}. For the type-T pylon, feature points of the part above the pylon body should also be considered. Calculate the geometric center of feature points of each layer of the pylon body. Normally, these center points are collinear. Therefore, calculate the average value of x coordinates and y coordinates of these geometric centers, respectively, to obtain x_{center}, y_{center}, and consider (x_{center}, y_{center},) as the geometric center of feature points of each layer above the pylon. Correct feature point coordinates of the part above the pylon body according to the following steps: keep the one which is farther from x_{center} between x_{maxi} and x_{mini}, and calculate the other according to the symmetry. For example, if $(x_{maxi} - x_{center}) > (x_{center} - x_{mini})$, $x'_{mini} = 2 \times x_{center} - x_{maxi}$. Similarly, correct the values of y_{maxi} and y_{mini}. As shown in Figure 15c,d (pink dots in blue circles), the feature points with wrong positions have been corrected.

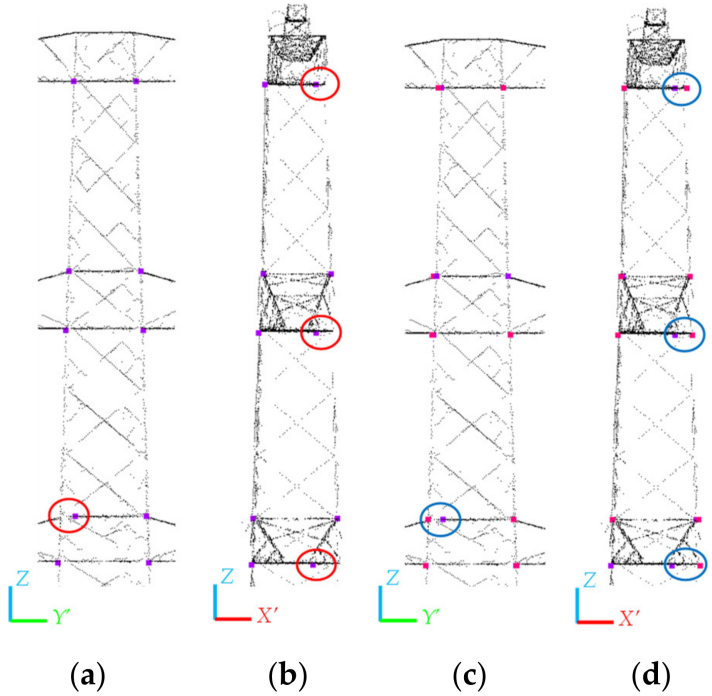

Figure 15. Correction of feature points: (**a**,**b**) uncorrected feature points of type-T pylon head, among which those in red circles are obvious wrong; (**c**,**d**) feature points of type-T pylon head before and after correction, represented in purple and pink, respectively.

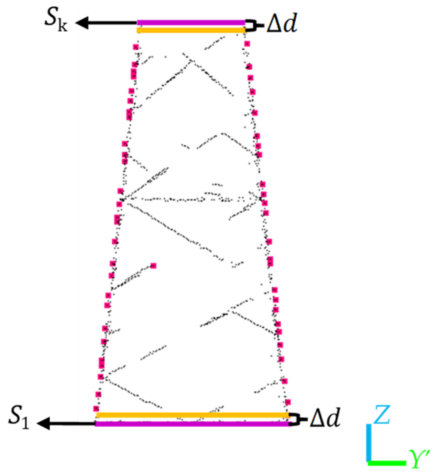

Figure 16. Boundary points of the pylon body.

3.3.3. Register Feature Point Sets

When the distance between the point cloud to be registered and the target point cloud is far, or there is a structural difference between them, direct fine registration is quick to fall into a local optimum [19], and it takes a long time. Therefore, several points are selected for registration. For each $component_i (i = 2, 3, \ldots)$ of the pylon, the feature points of the segmentation position S_i and S_{i+1} are taken as its feature point set P. Then the feature point set P is registered with the feature point set X of each component model in the model library in turn, and the transformation parameters including the scaling factor s, rotation matrix R, and translation matrix T are estimated during each iteration of the closest points (ICP).

The core of the ICP algorithm is to iteratively perform the following two steps until convergence. The first step is to search the corresponding point pairs between the point cloud to be registered and the target point cloud. The second one is to calculate the best

transformation between the corresponding point pairs and act on the point cloud to be registered [20,21]. The scale factor s is estimated within the ICP algorithm by the method proposed by Zinßer et al. [20]. In this study, the K-D tree nearest neighbor search algorithm is used to improve the searching efficiency of the corresponding point pairs. It should be noted that since the number of feature points of the uppermost component is less than that of the feature points of other components, one more step is added to scale the height of the component model according to the height of the component point cloud.

3.3.4. Pylon Reconstruction

For the pylon foot, it can be abstracted as the inverted triangular pyramid structure, which is relatively simple. Therefore, the pylon foot is planned to be directly reconstructed. In Figure 17, $P_{1i}(i = 1, 2, 3, 4)$ are feature points corresponding to the segmentation position S_1. $P_{1i}(i = 5, 6, 7, 8)$ are midpoints of four edges, which can be calculated by $P_{1i}(i = 1, 2, 3, 4)$. In addition, the X'Y' plane coordinates of $P_{0i}(i = 1, 2, 3, 4)$, whose Z coordinates are the minimum value of Z coordinate of the pylon, can be calculated by the line equations fitted in Section 3.3.2.

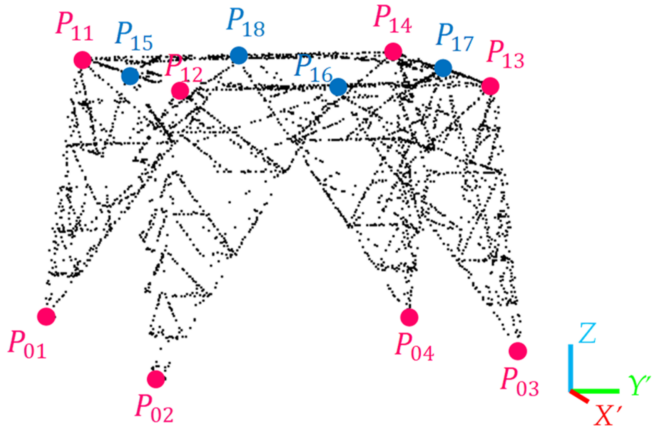

Figure 17. The pylon foot reconstruction.

For each component of pylon head and pylon body, the model matching method is adopted for reconstruction. The aligned point cloud $Cloud_{aligned}$, i.e., the point cloud sampled from the model in model library, is transformed according to Equation (4):

$$Cloud_{transform} = s \times R \times Cloud_{aligned} + T, \tag{4}$$

Calculate the distance between the original component point cloud and the component model point cloud transformed. The K-D tree is used to find corresponding point pairs between two point clouds mentioned before, and only the corresponding point pairs between whose distance is less than the distance T_d are recorded. For each component of one pylon, calculate RMSE of distance and amount of corresponding point pairs between it and each component model in the model library, which will be used to determine the best matching model and evaluate the accuracy of the results. The calculation formula of RMSE is shown in Equation (5):

$$RMSE = \sqrt{\frac{\sum_{i=1}^{n} d_i^2}{n}} \tag{5}$$

where d_i is the distance between the i-th pair of corresponding points, and n is amount of corresponding point pairs.

Find the maximum value of amount of corresponding point pairs, list the models whose number of point pairs is greater than the maximum value multiplied by the proportional threshold T_p as candidate models, and then select the component model with

the lowest RMSE; that is, the component model with the highest matching degree. Finally, combine the models of all components to complete 3D reconstruction of the pylon.

4. Results

The programs for power pylon structure segmentation and reconstruction were written in C++, and run on a laptop. Table 3 provides the configuration information of the laptop used.

Table 3. Laptop configuration information.

Laptop	CPU	GPU	RAM
Lenovo XiaoXin Pro 16ACH 2021	AMD Ryzen 7 5800H	NVIDIA GTX 1650	16 GB

The proposed method used to reconstruct six types of power pylon, and the parameter settings of the programs, are shown in Table 4.

Table 4. Parameters of the pylon reconstruction.

Parameter	Meaning	Value
H(m)	Minimum height of point cloud for redirection	(3/4) × height of the pylon
d_1(m)	The layer interval along the Z-axis direction	0.2
D(m)	The height of the sliding window W	2.0
d_2(m)	The grid interval when calculating horizontal fill rate	0.2
T_f	The threshold of horizontal fill rate	75%
T_α(°)	The angle threshold for identifying the key segmentation position	165
T_r	The proportional threshold for determining the segmentation position S_1	0.5
d_3(m)	The layer interval along the Y′-axis direction	0.2
d_s(m)	The sampling interval of the model	0.05
Δd(m)	The height parameter when extracting pylon body boundary points	0.2
T_d(m)	The distance threshold between corresponding point pairs	0.3
T_p	The proportional threshold of the amount of corresponding point pairs	90%

4.1. Accuracy of Feature Points

The segmentation result of the pylon is the basis of model matching, and feature points calculated based on the segmentation result directly affect the reconstruction accuracy. Eight parameters need to be set in the process of pylon segmentation and calculation of feature points. Missing pylon point cloud and noise points affect the parameter settings. The feature points of the pylon were extracted manually and compared with the calculated results, to evaluate the accuracy of the feature points. The comparison results are listed in Table 5.

Table 5. The result of precision verification about feature points extracted.

Pylon Number		S_1 cm	S_2 cm	S_3 cm	S_4 cm	S_5 cm	S_6 cm	S_7 cm	S_8 cm	Average (cm)
a	$\Delta x'_{min}$	4.2	9.9	0.6	1.2					4.0
	$\Delta x'_{max}$	2.4	6.1	3.8	5.2					4.4
	$\Delta y'_{min}$	6.1	0.8	1.1	1.3					2.3
	$\Delta y'_{max}$	0.4	1.8	9.1	4.1					3.8
	Δz	7.9	2.7	5.0	9.3					6.5
b	$\Delta x'_{min}$	3.8	9.5	1.7	2.2					4.3
	$\Delta x'_{max}$	1.8	4.4	5.0	0.7					3.0
	$\Delta y'_{min}$	3.6	0.7	7.2	3.1					3.6
	$\Delta y'_{max}$	6.3	3.2	3.7	2.7					4.0
	Δz	9.5	3.0	6.5	7.0					6.5

Table 5. *Cont.*

Pylon Number		S_1 cm	S_2 cm	S_3 cm	S_4 cm	S_5 cm	S_6 cm	S_7 cm	S_8 cm	Average (cm)
	$\Delta x'_{min}$	2.2	0.9	0.7	6.4					2.5
	$\Delta x'_{max}$	3.7	0.6	2.1	5.2					2.9
c	$\Delta y'_{min}$	4.0	0.3	0.5	0.9					1.4
	$\Delta y'_{max}$	0.4	3.0	0.6	2.9					1.7
	Δz	6.5	6.5	2.0	7.0					5.5
	$\Delta x'_{min}$	7.1	5.0	2.5	4.1	1.7	1.4	4.4	13.3	4.9
	$\Delta x'_{max}$	9.7	9.2	7.9	8.8	4.3	3.8	4.3	13.1	7.6
d	$\Delta y'_{min}$	2.0	3.7	1.6	2.0	1.8	7.9	9.8	13.1	5.2
	$\Delta y_{max'}$	1.2	0.9	2.5	5.1	1.2	1.7	0.9	0.5	1.8
	Δz	0.0	2.5	5.0	6.5	2.0	8.5	0.5	1.5	3.3
	$\Delta x'_{min}$	10.6	5.3	9.4	17.2	15.0	6.9	14.0		11.2
	$\Delta x'_{max}$	3.4	8.3	0.8	5.1	13.0	1.1	1.4		4.7
e	$\Delta y'_{min}$	2.1	6.5	5.0	9.6	2.6	1.4	0.8		4.0
	$\Delta y'_{max}$	0.7	12.0	11.7	1.6	15.1	18.7	13.1		10.4
	Δz	6.0	1.0	0.5	5.5	3.0	2.5	0.5		2.7
	$\Delta x'_{min}$	5.6	0.0	1.0	7.6	11.6				5.2
	$\Delta x'_{max}$	5.3	2.8	5.2	6.8	15.9				7.2
f	$\Delta y'_{min}$	6.4	1.0	3.8	6.5	0.0				3.6
	$\Delta y'_{max}$	1.5	0.9	0.9	9.1	1.0				2.7
	Δz	1.3	3.7	5.4	6.5	3.1				4.0

4.2. Accuracy of Pylon Reconstruction

Figure 18 shows the reconstruction results.

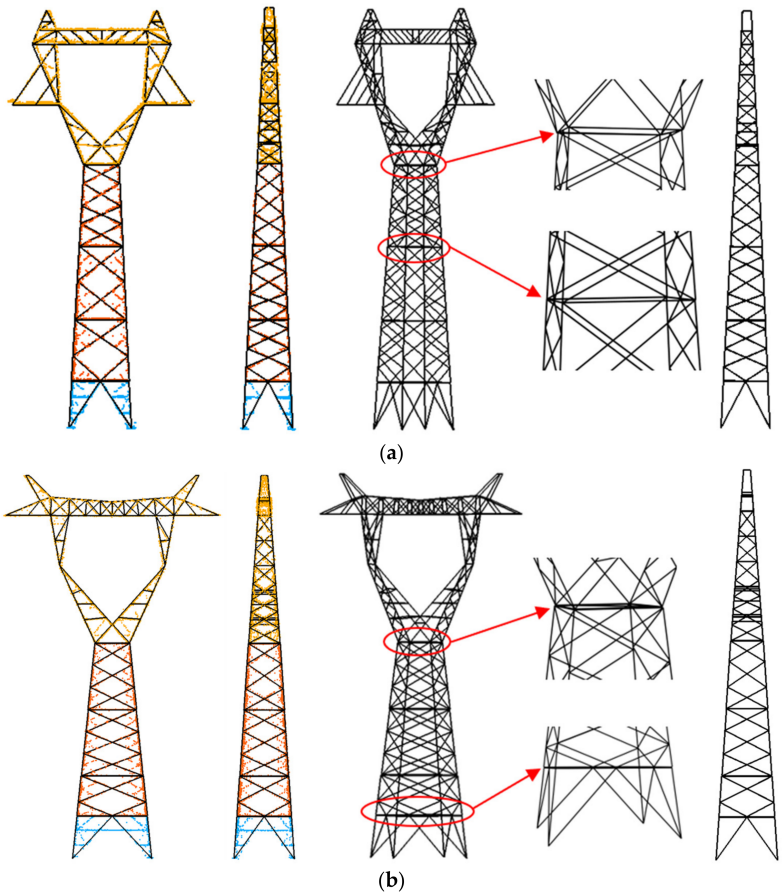

Figure 18. *Cont.*

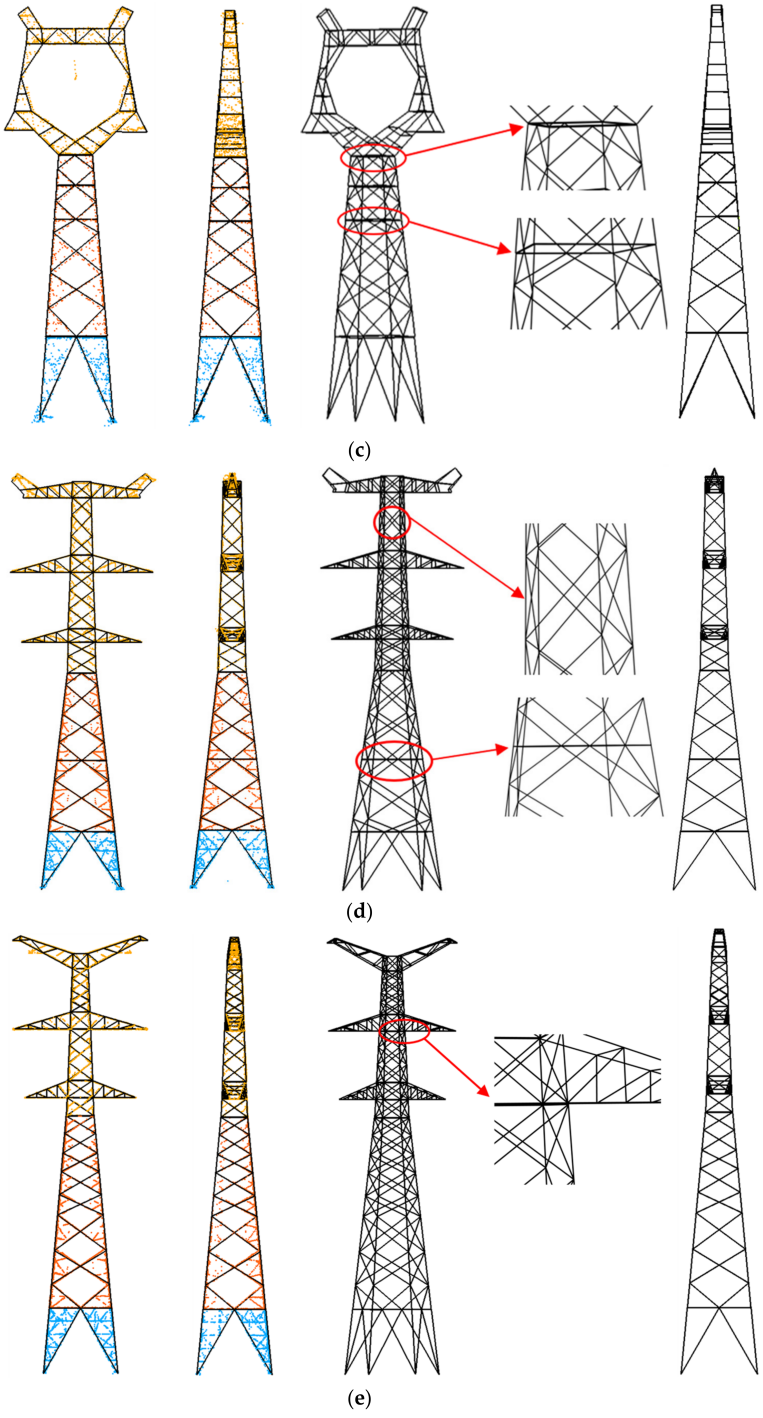

Figure 18. *Cont.*

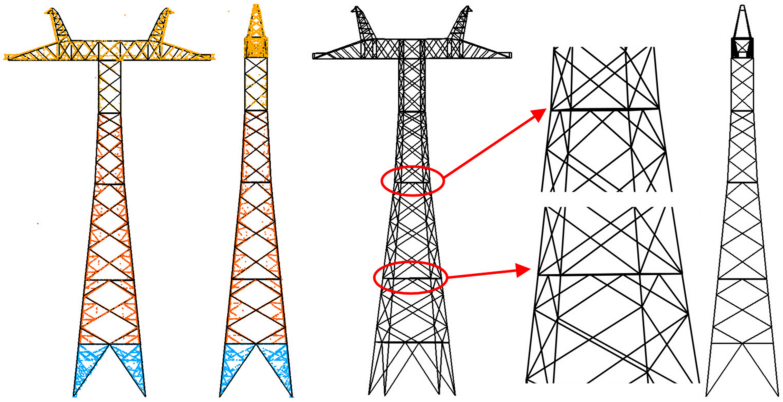

(**f**)

Figure 18. Pylon reconstruction results: (**a**–**f**) overlay display results of point cloud and model, as well as overall and magnification plots of the model, corresponding to pylon types a-f respectively.

Table 6 provides RMSE of the point distance between each component of pylon and the matched model. The average RMSE of all power pylon components in this study was 15.4 cm.

Table 6. Model matching results.

Pylon Number	C_1 * (cm)	C_2 * (cm)	C_3 * (cm)	C_4 * (cm)	C_5 * (cm)	C_6 * (cm)	C_7 * (cm)	C_8 * (cm)	C_9 * (cm)	Average (cm)
a	-	13.8	11.8	9.5	16.4					12.9
b	-	18.7	15.5	17.9	15.8					17.0
c	-	14.5	11.0	10.5	16.1					13.0
d	-	17.6	15.5	10.5	18.7	11.8	17.0	14.8	20.7	15.8
e	-	15.5	13.8	13.8	14.1	12.6	15.2	18.4		14.8
f	-	18.2	17.9	17.6	17.9	18.7				18.1

*C_i represents the $component_i$ of the pylon.

5. Discussion

The actual scanned point cloud usually has problems such as noise interference, data loss, and sparse density. It is necessary to prove the robustness of the proposed method to these factors.

5.1. Noise Impact

Noise points mainly exist in three areas of the pylon. There are insulator strings and power lines in the pylon head area, as shown in the black box area in Figure 19a. There may be high vegetation around the pylon body, as shown in the green box area in Figure 19a. The main interference items around the pylon foot are vegetation and ground points, as shown in the orange box area in Figure 19a. The noise points around the pylon body will affect the accuracy of feature points. As shown in Figure 19a (red dots), the position of feature points is deviated to the outside, which will cause the reconstructed model to be larger than the real model. Therefore, if such points exist, try to remove them as much as possible. Different from the type-O pylon, for the type-T pylon, noise points in the black box will cause the similar problem as mentioned above. The pylon foot reconstruction is based on the fitted edges of the pylon body, so the noise points around the foot have little impact. Figure 19b shows the result of pylon reconstruction after removing the noise points in the green box, which indicates its robustness to the other two types of noise.

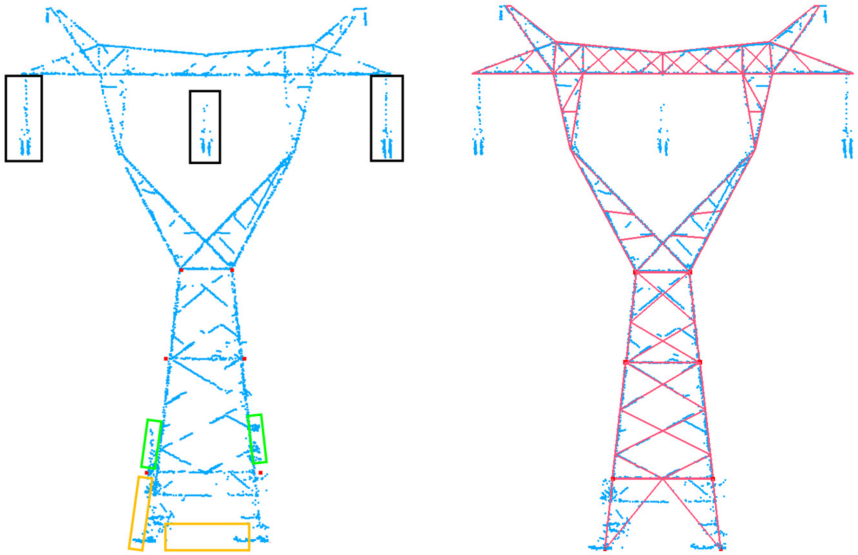

Figure 19. The impact of noise on pylon reconstruction: (a) the noise points around the pylon; (b) the result of pylon reconstruction after removing the noise points around the pylon body.

5.2. Data Loss

Due to occlusion during scanning, misclassification during classification and extraction, etc., point cloud data of pylon may be missing. As shown in Figure 20, from (a) to (i), from (j) to (o), the degree of data loss of the pylon head point cloud gradually deepens. In general, if corner points and height of the pylon head can be accurately obtained, and the pylon head retains some points, the corresponding model can be matched. Several points are missing in the middle part of the pylon body, but there are still a small number of boundary points. In this case, feature points can still be extracted and model matching can be performed, as shown in Figure 20p. Figure 20q shows the result of pylon reconstruction with data loss using the method proposed by Chen et al. [14]. Comparing Figure 20p,q, the model integrity of the former is stronger, which is a highlight of the model-driven strategy.

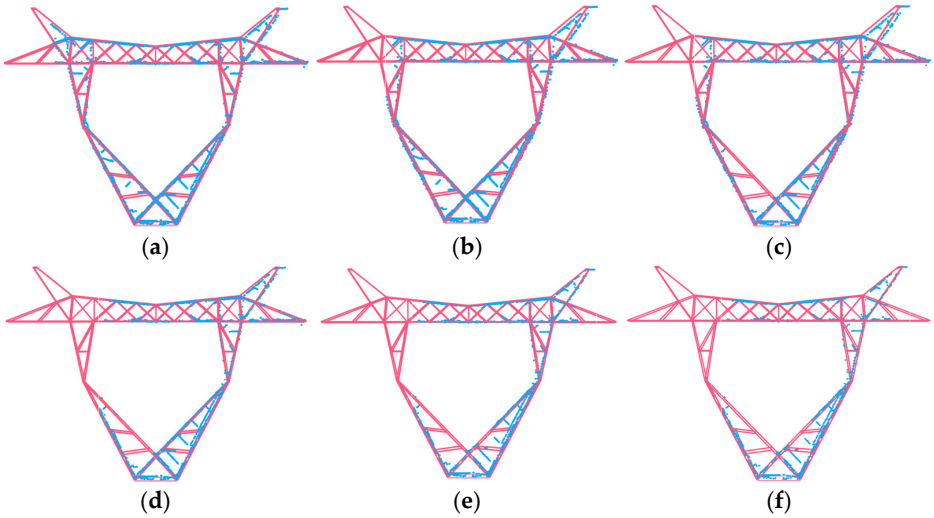

Figure 20. *Cont.*

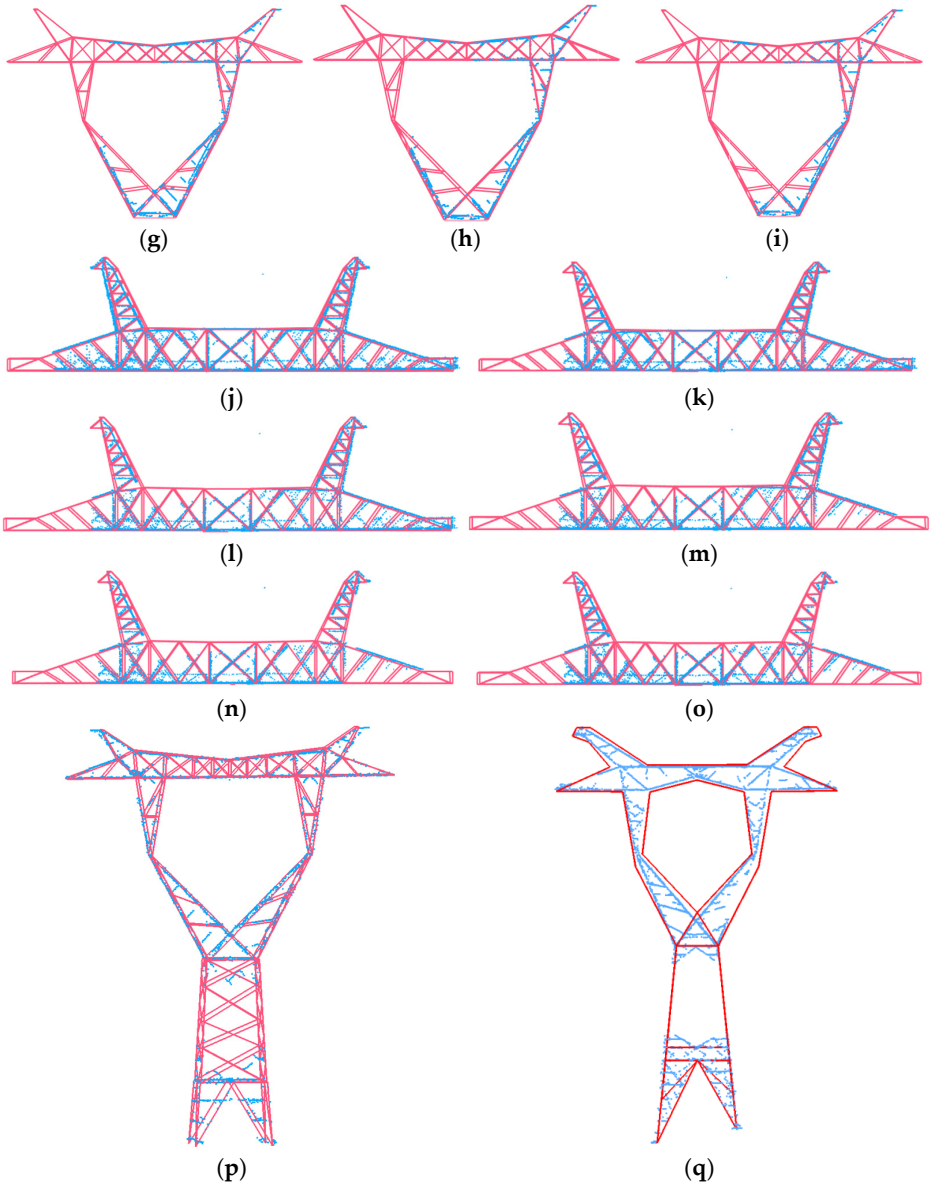

Figure 20. The results of pylon reconstruction with varying degrees of data loss: (**a**–**i**) type-O pylon head with data loss and 3D model; (**j**–**o**) type-T pylon head with data loss and 3D model; (**p**) pylon with data loss in body area and 3D model; (**q**) cited from Figure 29b of [14].

Since the method in this study strongly relies on the point cloud data of the segmentation positions, if the segmentation position point cloud is missing, it will have a great impact on the decomposition of the pylon. If the decomposition is wrong, it may match the model that is inconsistent with the actual situation, resulting in reconstruction failure.

5.3. Data Sparsity

LiDAR system usually emit a single line or multi-line laser during scanning. The points near one end of the laser rangefinder are densely arranged, and at the other end, the points which are far away from the laser rangefinder are sparse. To study the influence of data sparsity, the original point cloud data are uniformly sampled with distances varied from 0.1 m to 0.4 m, and specific sample information is shown in Table 7. When the sample distance is less than 0.4 m, the pylon usually can be reconstructed correctly. However, when the sample distance increases to 0.4 m, the point cloud becomes somewhat sparse. Due to improper parameter settings, segmentation position identification is prone to errors, as shown in Figure 21d.

Table 7. The number of pylon points uniformly sampled with different distances.

Pylon Number	Point Cloud		The Number of Points
a	Original Point Cloud		6163
	Sample distance	0.1 m	5069
		0.2 m	3590
		0.3 m	2573
		0.4 m	1955
b	Original Point Cloud		7489
	Sample distance	0.1 m	6565
		0.2 m	5318
		0.3 m	4173
		0.4 m	3288
f	Original Point Cloud		25,775
	Sample distance	0.1 m	23,106
		0.2 m	15,923
		0.3 m	11,528
		0.4 m	8663

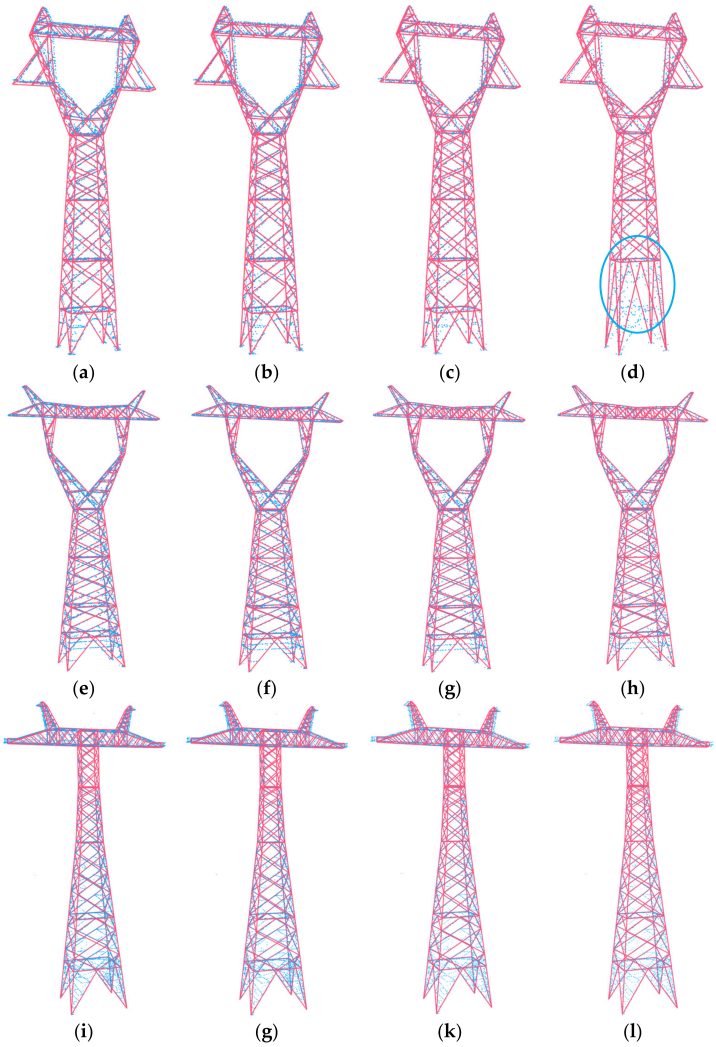

Figure 21. The results of pylon reconstruction with varying sample distances: (**a**,**e**,**i**) sample distance = 0.1 m; (**b**,**f**,**g**) sample distance = 0.2 m; (**c**,**g**,**k**) sample distance = 0.3 m; (**d**,**h**,**l**) sample distance = 0.4 m.

6. Conclusions

This study proposes an automatic reconstruction method for power pylons based on component segmentation and model matching, whose applicability and accuracy have been verified by experiments. The error in the segmentation position is less than 10 cm, and the average RMSE of all power pylon components in this study was 15.4 cm. Compared to the existing pylon reconstruction methods, our proposed method has the following several characteristics and merits: (1) it considers the graphical characteristics, i.e., concavity vs. convexity, as a new feature to effectively identify the key segmentation position of the power pylon; (2) it automatically extracts and corrects the pylon feature points, and registers the corresponding feature point pairs; (3) due to occlusion during scanning, misclassification during classification and extraction, etc., it is one of the common situations in which some data of the acquired point cloud is lost. The model-driven strategy is adopted in this study, and complete models can still be reconstructed for some power pylons with missing data; and (4) it has high robustness to the noise points around the pylon head and foot. In short, our method is effective for power pylon visualization and digitization, ensuring the integrity of the reconstructed model. Constructing 3D vector models can not only restore true forms of main facilities of the transmission line, but also facilitate the detection of faults in time to then take measures. At the same time, it is also convenient in planning surrounding houses, buildings, etc.

Despite these capabilities, some parts need improvement, which will be addressed in future studies: (1) under normal circumstances, the pylon is left-right symmetrical. Hence, if the missing parts are not symmetrical in distribution and they fall into a small area, this feature can be used to supplement the missing part data. (2) It should be noted that model-driven strategy is limited by the existing model library, which needs to be expanded. (3) Extracting more feature points to ensure reconstruction accuracy and improve matching efficiency should also be considered.

Author Contributions: Conceptualization, Y.Q. and X.X.; Data curation, X.X. and P.W.; Formal analysis, P.W. and C.W.; Funding acquisition, S.N.; Investigation, X.X., S.N. and H.G.; Methodology, Y.Q., X.X. and P.W.; Project administration, P.W.; Resources, P.W. and H.G.; Software, Y.Q.; Supervision, S.N.; Validation, Y.Q.; Visualization, Y.Q. and X.X.; Writing—original draft, Y.Q.; Writing—review and editing, X.X., P.W., H.G. and C.W. All authors have read and agreed to the published version of the manuscript.

Funding: This research was funded by [National Key R&D Program of China] under Grant [number 2021YFF0704600] and [the Youth Innovation Promotion Association Chinese Academy of Sciences] under Grant [number 2019130].

Acknowledgments: We would like to thank all the anonymous reviewers and editors for many constructive comments and suggestions on the manuscript.

Conflicts of Interest: The authors declare no conflict of interest.

References

1. Zhou, R.; Jiang, W.; Jiang, S. A novel method for high-voltage bundle conductor reconstruction from airborne LiDAR data. *Remote Sens.* **2018**, *10*, 2051. [CrossRef]
2. Qiao, S.; Sun, Y.; Zhang, H. Deep learning based electric pylon detection in remote sensing images. *Remote Sens.* **2020**, *12*, 1857. [CrossRef]
3. Peng, X.; Song, S.; Qian, J.; Chen, C.; Wang, K.; Yang, Y.; Zheng, X. Research on automatic positioning algorithm of power transmission towers based on UAV LiDAR. *Power Syst. Technol.* **2017**, *41*, 3670–3677. [CrossRef]
4. Yu, B.; Chen, F.; Xu, C. Landslide detection based on contour-based deep learning framework in case of national scale of Nepal in 2015. *Comput. Geosci.* **2020**, *135*, 10438. [CrossRef]
5. Chen, L. Analysis of transmission line real-time monitoring technology in power system. *Electron. Compon. Inf. Technol.* **2020**, *4*, 82–83. [CrossRef]
6. Ma, W.; Wang, J.; Wang, C.; Xi, X.; Wang, P. Precise extraction and reconstruction of power line by using model residual. *Sci. Surv. Mapp.* **2020**, *45*, 60–66. [CrossRef]
7. Guo, B.; Huang, X.; Li, Q.; Zhang, F.; Zhu, J.; Wang, C. A stochastic geometry method for pylon reconstruction from airborne LiDAR data. *Remote Sens.* **2016**, *8*, 243. [CrossRef]

8. Zhou, R.; Jiang, W.; Huang, W.; Xu, B.; Jiang, S. A heuristic method for power pylon reconstruction from airborne LiDAR data. *Remote Sens.* **2017**, *9*, 1172. [CrossRef]
9. Chen, Z.; Lan, Z.; Long, H.; Hu, Q. 3D modeling of pylon from airborne LiDAR data. In Proceedings of the 18th China National Symposium on Remote Sensing-Remote Sensing of the Environment, Wuhan, China, 20–23 October 2012. [CrossRef]
10. Huang, W.; Jiang, S.; Jiang, W. A model-driven method for pylon reconstruction from oblique UAV images. *Remote Sens.* **2020**, *20*, 824. [CrossRef] [PubMed]
11. Xiao, Y.; Wang, C.; Xi, X.; Wang, F. 3D building model reconstruction from airborne LiDAR data. *Sci. Surv. Mapp.* **2014**, *39*, 37–41. [CrossRef]
12. Lin, X.; Duan, M.; Zhang, J.; Zang, Y. A method of reconstructing 3D powerlines from airborne LiDAR point clouds. *Sci. Surv. Mapp.* **2016**, *41*, 109–114+64. [CrossRef]
13. Chen, J.; Wang, X.; Lu, X.; Zhang, C.; Wang, W.; Wang, R.; Shen, X. The overviews of application of three-dimensional LiDAR technology in operation and maintenance of overhead transmission lines in China. In Proceeding of the 2013 3rd International Conference on Advanced Measurement and Test (AMT 2013), Xiamen, China, 13 March 2013. [CrossRef]
14. Chen, S.; Wang, C.; Dai, H.; Zhang, H.; Pan, F.; Xi, X.; Yan, Y.; Wang, P.; Yang, X.; Zhu, X.; et al. Power pylon reconstruction based on abstract template structures using airborne LiDAR data. *Remote Sens.* **2019**, *11*, 1579. [CrossRef]
15. Han, W. Three-dimensional power tower modeling with airborne LiDAR data. *J. Yangtze River Sci. Res. Inst.* **2012**, *29*, 122–126. [CrossRef]
16. Liu, C.; Sun, S.; Zhao, L. A lightweight network for power tower extraction from laser point cloud. *Laser Technol.* **2021**, *45*, 367–372. [CrossRef]
17. Yu, W.; Xi, J.; Lei, W.; Wu, Z.; Wang, H.; Zhu, C.; Zhong, H.; Tang, T. A model-driven 3D modeling of power transmission towers. *Geomat. World* **2020**, *27*, 127–132.
18. Li, Q.; Chen, Z.; Hu, Q. A model-driven approach for 3D modeling of pylon from airborne LiDAR data. *Remote Sens.* **2015**, *7*, 11501–11524. [CrossRef]
19. Peng, Z.; Lü, Y.; Qu, C.; Zhu, D. Accurate registration of 3D point clouds based on keypoint extraction and improved iterative closest point algorithm. *Laser Optoelectron. Prog.* **2020**, *57*, 68–79. [CrossRef]
20. Zinßer, T.; Schmidt, J.; Niemann, H. Point set registration with integrated scale estimation. In Proceeding of the International conference on pattern recognition and image processing, Minsk, Belarus, 18–20 May 2005.
21. He, Y.; Liang, B.; Yang, J.; Li, S.; He, J. An iterative closest points algorithm for registration of 3D laser scanner point clouds with geometric features. *Remote Sens.* **2017**, *17*, 1862. [CrossRef] [PubMed]